

Arsenate removal on the ion exchanger modified with cerium(III) ions

Sebastian Dudek, Dorota Kołodyńska

¹ Department of Inorganic Chemistry, Institute of Chemical Sciences, Faculty of Chemistry, Maria Curie-Skłodowska University, Maria Curie-Skłodowska Sq. 2, 20-031 Lublin, Poland.

Corresponding author: sebastian.dudek@mail.umcs.pl (Sebastian Dudek)

Abstract: The iron oxide ion exchanger Ferrix A33E was successfully modified with cerium(III) ions to obtain Ferrix A33E-Ce(III) providing much better sorption properties in relation to the As(V) species. The new material has been characterized using a number of techniques including scanning electron microscopy SEM, nitrogen adsorption/desorption isotherms, Fourier transform infrared spectroscopy FTIR and X-ray photoelectron spectroscopy XPS. At optimal pH 6 the main mechanism of arsenate adsorption on A33E-Ce(III) was electrostatic attraction and formation of monodentate and bidentate surface complexes. The process was exothermic and spontaneous. Unlike the unmodified ion exchanger, A33E-Ce(III) could completely remove arsenic from the arsenate solution at a concentration of 50 mg/dm³ in 60 minutes. Furthermore, the maximum sorption capacity for As(V) was determined to be 60.41 mg/g which almost doubled after modification with cerium(III) ions. It is also worth noting that even after three cycles of sorption/desorption A33E-Ce(III) exhibited a higher sorption capacity than unmodified A33E before the arsenate adsorption. It can be concluded that modifying the sorbent with a small amount of cerium(III) ions boosts its sorption properties significantly, improves effectiveness of water purification and reduces the overall operation cost.

Keywords: arsenic, adsorption, cerium, iron oxides, Ferrix A33E

1. Introduction

Arsenic contamination in groundwater at elevated concentrations is reported in many countries around the world, e.g. Argentina, Bangladesh, Chile, China, India, Mexico (Hao et al., 2018). The main reasons for this phenomenon include industrial activities, weathering of rocks, geochemical reactions, volcanic emissions and biological activities (Chowdhury and Mulligan, 2011). The arsenic polluted groundwater was used for underdeveloped or developing countries without treatment, which led to various detrimental health effects (including lung cancer, cardiovascular diseases and skin disorders) in the local population (Podgorski et al., 2017). Therefore, the development of an effective method of water purification is of great importance.

Numerous technologies have been elaborated on arsenic removal from aqueous solutions based on various treatment methods (Adeloju et al., 2021). Among these technologies, adsorption seems to demonstrate the greatest potential due to its cost effectiveness, maintenance, versatility and simplicity of operation. Extremely common adsorbents designed to remove arsenic are those based on iron oxides (Siddiqui and Chaudhry, 2017) or also hybrid materials combining iron and other metals including titanium (Gupta and Ghosh, 2009), zirconium (Chaudhry et al., 2017), aluminium (Maji et al., 2018), copper (Zhang et al., 2013). Recently, some papers on the materials containing rare earth elements REE have also been presented (Shi et al., 2015; Yu et al., 2017; Lingamdinne et al., 2019; Dudek and Kołodyńska, 2020; T. Liang et al., 2020; Wang et al., 2020). The metal oxide/hydroxide, metal oxide/hydroxide modified adsorbents, and the metal ion impregnated adsorbents are the most common types of such novel materials. The unusual physicochemical properties of REEs, as well as their exceptional arsenic removal efficiency, have piqued the interest of researchers. It is believed that the multiple-species REE adsorbents exhibit larger arsenic sorption capacity, greater stability and are cheaper compared to the single-species REE materials (Yu et al., 2018). Through ligand exchange, complex formation, and electrostatic interactions, various functional groups on the adsorbent surface

can play a significant role in the adsorption process (Muthu Prabhu et al., 2018). Loading the REE oxides/hydroxides or REE ions onto the porous materials characterized by a large surface area and great porosity may also lead to the increase of adsorption rate (Yu et al., 2018).

As REEs are relatively expensive, it is advantageous to combine them with readily accessible and less expensive metals (e.g., aluminium, iron, manganese) to create a new series of composites as adsorbents that retain the advantages of REEs while reducing overall costs (S. Liang et al., 2020; Muthuselvi et al., 2021). Therefore, in this study the modification of the commercially available iron oxide ion exchanger Ferrix A33E (containing the quaternary ammonium groups) was made using cerium(III) ions. There is no report in the literature about Ce(III)-modification of an iron-based sorbent with the quaternary ammonium groups. The main objectives of the research were (1) modification of Ferrix A33E with Ce(III) ions (2) characterization of the newly obtained material and (3) investigating the arsenate(V) adsorption process and comparing the sorption efficiency on the modified and unmodified ion exchangers.

2. Materials and methods

2.1. Sorbent modification and characterization

The Ce(III) solution of the concentration 1000 mg/dm^3 was prepared by dissolving the proper amount of cerium(III) nitrate hexahydrate $\text{Ce}(\text{NO}_3)_3 \cdot 6\text{H}_2\text{O}$ (Sigma Aldrich, USA) in distilled water. The solution was then diluted to 100 mg/dm^3 and the pH was adjusted to 4 by adding the proper amount of 1M NaOH (Chempur, Poland). The portions of 0.5 g of A33E (Purolite, USA) were inserted in 500 cm^3 conical flasks and 100 cm^3 of the previously prepared Ce(III) solution of the concentration of 100 mg/dm^3 was added to each of them. The samples were then shaken under the following conditions: time 6 hours, shaking speed 180 rpm and temperature 295 K. In the next step, the sorbent was removed from the solution by gravity filtration and dried at 333 K for 24 hours. As a result there was developed the modified A33E-Ce(III) sorbent, which was then examined for characterisation and removal of arsenic(V) ions.

To assess the surface morphology, including surface features, scanning electron microscopy (SEM) (Quanta 3D FEG, FEI, USA) with an extended depth of field (EDF) function was utilized. The pictures of SEM A33E and A33E-Ce(III) were compared. Images of the surface of A33E-Ce(III) following the As(V) ion sorption were also taken.

The nitrogen adsorption/desorption isotherms at 77 K (ASAP 2405, Micromeritics, USA) were used to study the morphological characteristics of A33E, A33E-Ce(III), and A33E-Ce(III)-As(V) following the preliminary degassing of the samples at the specified temperature. To calculate the specific surface area, the Brunauer, Emmett, and Teller (BET) technique was used. The Barret-Joyner-Halenda model was also applied to compute total pore volumes and average pore diameters.

The point of zero charge (pH_{pzc}) of A33E and A33E-Ce(III) was determined using the drift technique (Jiao et al., 2017). The pH_{pzc} was calculated by varying the pH of 20 cm^3 0.01 M NaCl from 2 to 11 (pH_i). 0.1 g of A33E or A33E-Ce(III) was added into the flask, shaken for 6 hours and then the final pH_f was determined. The pH_{pzc} value is the point at which $\text{pH}_i - \text{pH}_f = 0$. The pH was measured with a Radiometer PHM 84 pH meter (Denmark) with glass REF 451 and calomel pHG 201-8 electrodes.

The spectra of the studied adsorbents were acquired using infrared spectroscopy with the Fourier transformation (FTIR). The attenuated total reflection technique was used to evaluate A33E and A33E-Ce(III) before and after the As(V) adsorption using the Nicolet 8700A spectrometer (Thermo Scientific, USA). As a result, the specified functional groups on the material surface could be identified. The FTIR spectra were collected in the wavenumber range of $4000\text{--}400 \text{ cm}^{-1}$.

The X-ray photoelectron spectroscopy XPS was used to investigate the composition and valence state of the elements included in A33E and A33E-Ce(III) before and after the arsenate(V) ion uptake (Prevac, Poland).

2.2. Batch experiments

To determine the pH effect on As(V) adsorption efficiency on experiment was conducted in 100 cm^3 flasks. The A33E-Ce(III) samples weighing 0.1 g were placed in the flasks containing 20 cm^3 of arsenate(V) solution at the concentration of 100 mg/dm^3 . The pH range was set from 4 to 11 by adding

the appropriate amounts of 0.01M NaOH or 0.01M HCl. The flasks were then shaken for 360 minutes with the laboratory shaker Elpin+ type 357 (Elpin Plus, Poland). The gravity filtration was used to separate A33E-Ce(III) from the solution. The concentration of arsenate(V) ions was determined using the spectrophotometric method (Cary 60, Agilent Technologies, USA), which involved the formation of complexes with ammonium molybdate and the absorbance measurement at 870 nm. Eq. 1 was used to calculate the adsorption capacity of As(V) ions (Badruddoza et al., 2013):

$$q_t = (c_0 - c_t) \times \frac{V}{m} \quad (1)$$

where: q_t is the amount of As(V) adsorbed at time t (mg/g), c_0 denotes the initial concentration of As(V) in the solution (mg/dm³), c_t represents the concentration of As(V) in the solution after time t (mg/dm³), V is the volume of the solution containing As(V) ions (dm³) and m symbolizes the mass of ion exchanger (g).

Additionally, the sorption percentage was calculated using Eq. 2 (Yetilmezsoy et al., 2020):

$$\%S = \frac{(c_0 - c_t)}{c_0} \times 100\% \quad (2)$$

Batch experiments were also conducted to investigate the kinetics of arsenate(V) adsorption at the initial As(V) concentrations of 25, 50, and 100 mg/dm³ and pH 6. A33E-Ce(III) samples weighing 0.1 g were prepared in 100 cm³ conical flasks and 20 cm³ As(V) solutions were added to be shaken for the specified time – between 1 and 360 minutes (temperature 295 K, shaking speed 180 rpm). Eqs. 1 and 2 were used to calculate the adsorption capacities and sorption percentages. The kinetics of arsenate(V) adsorption onto A33E-Ce(III) was studied using the pseudo-first order (PFO), pseudo-second order (PSO), Elovich, and intraparticle diffusion (IPD) models. The models applicability was assessed using the error analysis – determination coefficient (R^2), the sum of squared errors (SSE) and F-test. The pseudo-first-order (PFO) kinetic model was developed by Lagergren and Ho to explore sorption in the liquid-solid systems. It is described by Eqs. 3 and 4 presenting the linear form (Xiong et al., 2021):

$$\frac{dq_t}{dt} = k_1(q_e - q_t) \quad (3)$$

$$\ln(q_e - q_t) = \ln q_e - k_1 t \quad (4)$$

where: q_t represents the quantity of As(V) adsorbed onto the adsorbent at time t (mg/g), q_e denotes the equilibrium adsorption capacity (mg/g), k_1 is the PFO rate constant (1/min).

The PSO Eq. is built on the concept that the rate of adsorption is a quadratic function of the difference between the equilibrium adsorption capacity and the adsorption capacity after time t . Eqs. 5 and 6 represent the non-linear and linear forms of PSO model, respectively (Guo and Wang, 2019):

$$\frac{dq_t}{dt} = k_2(q_e - q_t)^2 \quad (5)$$

$$\frac{t}{q_t} = \frac{1}{k_2 q_e^2} + \frac{t}{q_e} \quad (6)$$

where: k_2 indicates the PSO rate constant (g/(mg·min)).

The Elovich model presupposes an energetically heterogeneous solid surface and a chemisorption process. Eqs. 7 and 8 reflect the non-linear and linear variants of the Elovich model, respectively (Ali et al., 2019):

$$\frac{dq_t}{dt} = \alpha \exp^{-\beta q_t} \quad (7)$$

$$q_t = \frac{1}{\beta} \ln(\alpha\beta) + \frac{1}{\beta} \ln t \quad (8)$$

where: α represents the initial adsorption rate (mg/(g·min)) and β is related to the surface coverage and chemisorption activation energy (g/mg).

If the adsorption process is regulated by intraparticle diffusion, the plot of q_t versus the square root of time (\sqrt{t}) should be linear according to the intraparticle diffusion IPD model represented by Eq. 9 (Ravi and Pandey, 2019):

$$q_t = k_i \sqrt{t} + C \quad (9)$$

where: k_i signifies the IPD rate constant and C is the boundary layer thickness.

In the case of equilibrium and thermodynamic studies As(V) solutions with different initial concentrations (25 – 1000 mg/dm³) were made and their pH was adjusted to 6 before the use. Adsorption experiments were performed at various temperatures: 295 K, 313 K, 333 K and a shaking

speed of 180 rpm. All tests were carried out with the established parameters, i.e. 6-hour contact time, the same adsorbent dosage and adsorbate volume as for the study of pH effect on the adsorption efficiency and kinetics. In order to fit the experimental data four isotherm models were used. The Langmuir (Eq. 10), Freundlich (Eq. 11), Dubinin-Radushkevich (Eqs. 12, 13, 14) and Redlich-Peterson (Eq. 15) models non-linear forms are shown below (Bergmann and Machado, 2015; Zhang and Leiviskä, 2020):

$$q_e = \frac{q_m K_L c_e}{1 + K_L c_e} \quad (10)$$

where: q_e represents the sorption capacity at equilibrium (mg/g), c_e indicates the equilibrium solute concentration (mg/dm³), q_m (g/mg) and K_L (dm³/mg) denotes the Langmuir constants related to the maximum sorption capacity and the sorption energy, which were calculated from the slope and intercept of the linear plot c_e/q_e vs c_e ;

$$q_e = K_F c_e^n \quad (11)$$

where: K_F (mg/g) and n (-) denote the constants related to the adsorption capacity and adsorption intensity, respectively. They can be obtained from the slope and intercept of the plot $\log q_e$ vs $\log c_e$;

$$q_e = q_{DR} e^{-K_{DR} \varepsilon^2} \quad (12)$$

$$\varepsilon = RT \ln \left(1 + \frac{1}{c_e} \right) \quad (13)$$

$$E = \frac{1}{\sqrt{2\beta}} \quad (14)$$

where: q_{DR} (mol/g) signifies the theoretical adsorption capacity, β (mol²/J²) represents the activity constant related to the mean free energy of adsorption, ε corresponds to the Polanyi potential, R (8.314 J/K/mol) represents the gas constant, T (K) denotes the temperature, E (J/mol) is related to the required energy to transfer a mole of sorbate from the solution to the sorbent surface.

$$q_e = \frac{K_{RP} c_e}{1 + a_{RP} c_e^g} \quad (15)$$

where: K_{RP} (dm³/g) and a_{RP} (dm³/mg)^g denote the Redlich-Peterson constants; g represents an exponent whose value must be between 0 and 1.

Temperature effects on the As(V) ion adsorption on A33E-Ce(III) were also examined, and major thermodynamic parameters were calculated using Eqs. 16, 17 and 18 (Hu et al., 2015):

$$K_d = \frac{q_e}{c_e} \quad (16)$$

$$\Delta G^0 = -RT \ln K_d \quad (17)$$

$$\ln K_d = -\frac{\Delta H^0}{RT} + \frac{\Delta S^0}{R} \quad (18)$$

where: K_d (dm³/g) represents the distribution coefficient, ΔG^0 (kJ/mol) denotes the change of Gibbs energy, ΔH^0 (kJ/mol) signifies the change of enthalpy and ΔS^0 (kJ/mol·K) is related to the entropy.

To assess the reusability of A33E-Ce(III), 0.1 g of the ion exchanger was put into three 100 cm³ flasks, and 20 cm³ of As(V) solution of 100 mg/dm³ and pH 6 was added to each of them. The samples were shaken for 6 hours at the temperature 295 K and the shaking speed 180 rpm. In the next step, the sorbent was removed from the solution by gravity filtration and dried at 333 K for 24 hours. The dry samples were re-placed in the 100 cm³ flasks and 20 cm³ of NaOH solutions at 0.05, 0.2, and 1M concentrations was added to them. The samples were also shaken for 6 hours (temperature 295 K, shaking speed 180 rpm). Following that, the adsorbent was removed from the solution by filtration and dried at 333 K for 24 hours. The experiment was conducted twice more with 1M NaOH. The concentration of As(V) ions in the solution was measured after each adsorption and desorption step.

3. Results and discussion

3.1. Sorbent characterization

SEM was utilized to analyse the morphological properties of A33E, A33E-Ce(III) and A33E-Ce(III)-As(V) (A33E-Ce(III) after the arsenate adsorption). The all images are presented in Fig. 1. Zhang et al. presented three forms of cerium oxide morphologies, i.e. nanorods (Ce-R), nanoparticles (Ce-P) and nanoflakes (Ce-F) (Zhang et al., 2016). Each morphology can be obtained using a different method of material preparation. In this study, modification with Ce(III) ions resulted in the increased

heterogeneity and the formation of nanoflakes (Ce-F) on the A33E surface. Numerous pores of varied sizes could facilitate the adsorption of As(V) ions at the active sites. Furthermore, backscattered electron (BSE) imaging was employed to detect particles containing heavier elements, such as REEs, that appeared brighter in the SEM-BSE images (Xu et al., 2019). The bright spots in Fig. 2 are related to the adsorbed cerium(III) ions, indicating that A33E was successfully modified. The arsenate adsorption on A33E-Ce(III) resulted in pores filling with As(V) ions and reduction of the surface heterogeneity (Fig. 1 g, h, i).

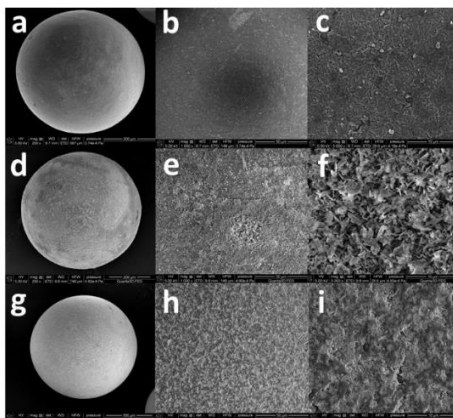


Fig. 1. SEM images of A33E (a-c), A33E-Ce(III) (d-f) and A33E-Ce(III)-As(V) (g-i) at the magnifications 150 x (g), 200 x (d), 250 x (a), 1000 x (b, e, h) and 5000 x (c, f, i)

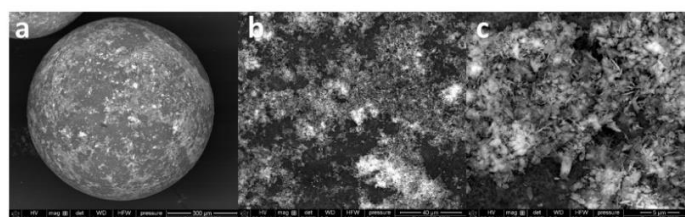


Fig. 2. SEM images of A33E-Ce(III) taken using the BSE detector at the magnifications 150 x (a), 1000 x (b) and 5000 x (c)

Using the N₂ adsorption-desorption technique, the specific surface areas, pore volumes, and average pore diameters of A33E, A33E-Ce(III), and A33E-Ce(III)-As(V) were determined. The variations in the materials specific surfaces were minor. They increased from 53.12 (Dudek and Kołodyńska, 2021) to 56.72 m²/g after modification, and reached 60.71 m²/g following the As(V) sorption. The total pore volume also increased in the order of A33E, A33E-Ce(III), A33E-Ce(III)-As(V) and was equal to 0.122, 0.125 and 0.140 cm³/g, respectively. According to the IUPAC classification all the presented isotherms (Fig. 3) are of type IV and include the H3 hysteresis loops which suggests that the mesoporous structure is formed by the slit-like mesopores (Allothman, 2012; Xiao et al., 2018). The mesoporous nature of the tested materials was also proved by the presented pore distribution (Fig. 3). It can be noticed that the size of pores exhibits a strong peak between 2.0 nm and 50 nm. There were no significant changes in the average pore diameter. After the modification with cerium(III) ions, there was a decrease from 9.18 to 8.80 nm, and after the adsorption of As(V), it increased to 9.22 nm.

It is well known that solution pH affects the surface charge of adsorbents, the dissociation of functional groups on the adsorbent active sites and the degree of ions ionization in the solution (Komnitsas et al., 2017). Inorganic arsenic(V) acid creates deprotonated anionic species in municipal waters with a pH of 6.5-8.5 (Reid et al., 2020; Bhandari et al., 2021). The previous study revealed that the pHPZC for A33E is 8.29 (Dudek and Kołodyńska, 2021), however, the value for A33E-Ce(III) is smaller and approaches 8.12 (Fig. 4). Given that the pHPZC of the A33E-Ce(III) surface is 8.12, it is clear that a negative charge occurs on its surface at pH above pHPZC and a positive charge forms at pH below that value (Dutta et al., 2004). As a result, adsorption of arsenate anions on the surface of A33E-Ce(III) is

expected to be preferred for the solution pH values smaller than 8.12 where greater electrostatic attraction may occur.

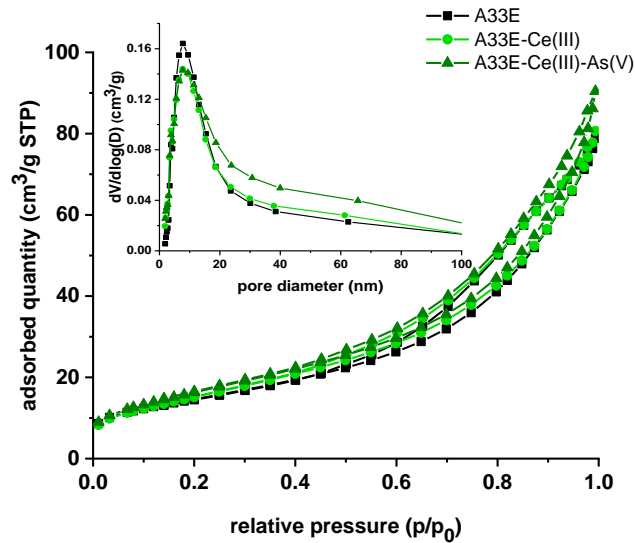


Fig. 3. N₂ adsorption/desorption isotherms of A33E (black), A33E-Ce(III) (light green) and A33E-Ce(III)-As(V) (dark green). The inset image shows the pore distribution of the tested materials

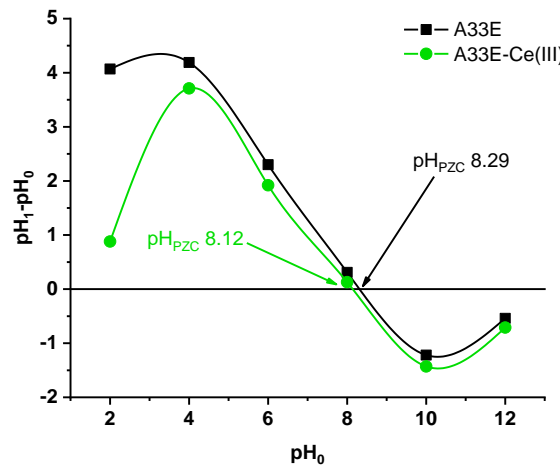


Fig. 4. Points of zero charge of A33E (black) and A33E-Ce(III) (green)

The FTIR analysis was used to determine changes in the functional groups and chemical bonds in A33E and A33E-Ce(III) before and after the As(V) adsorption (Fig. 5). The broad band observed between 3650 and 3100 cm⁻¹ centered around 3200 cm⁻¹ is attributed to the O-H stretching vibrations derived from the physisorbed water (Mino et al., 2020). The bands at 3030 cm⁻¹ and 2920 cm⁻¹ relate to polystyrene crosslinked with divinylbenzene and correspond to the vibrations of aromatic C-H and aliphatic C-H, respectively (Shin et al., 2015). The quaternary ammonium group -NR₄⁺ and H-O-H bending vibrations can be attributed to the double peak at 1636 and 1613 cm⁻¹ (Wang et al., 2009; Mino et al., 2020). Additionally, the band at 1480 cm⁻¹ also belongs to the -NR₄⁺ group and becomes less intense as a result of the Ce(III) and As(V) adsorption (Valdés et al., 2018). The spectra after the As(V) adsorption revealed the appearance of a new peak at 865 cm⁻¹ that was not present before adsorption. Most likely this peak indicates the formation of an As-O bond, which is consistent with the previous research results (T. Liang et al., 2020). Moreover, the peak for A33E-Ce(III)-As(V) is more intense than that of A33E-As(V) suggesting that the mechanism of arsenate adsorption could be different. In the case of A33E-Ce(III)-As(V) a new peak is observed at 448 cm⁻¹. It can be attributed to the Ce-O-As bond, just as the La-O-As vibration band at 445 cm⁻¹ in the lanthanum arsenate (Wang et al., 2020). This is due to the bonding formation between the cerium active sites and the oxygen atoms of arsenate(V). These findings point out to the formation of inner-sphere surface complexes.

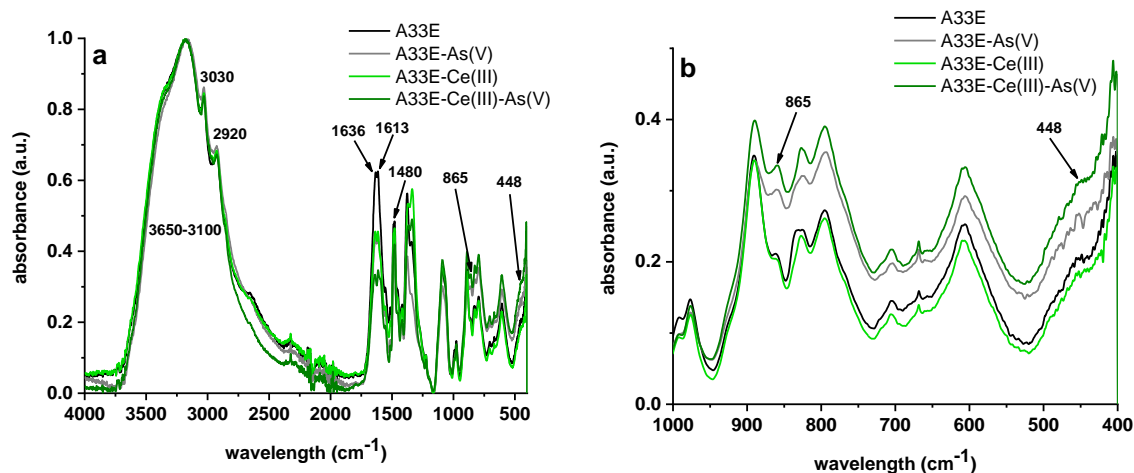


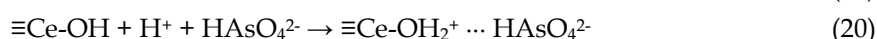
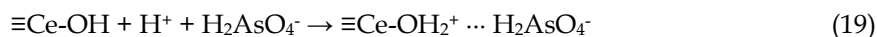
Fig. 5. FTIR spectra of A33E (black), A33E after the As(V) adsorption (grey), A33E-Ce(III) (light green) and A33E-Ce(III) after the As(V) adsorption (dark green) in the range of 4000-400 cm^{-1} (a) and 1000-400 cm^{-1} (b).

The surface elemental composition and the oxidation states of the elements were analysed by X-ray photoelectron spectroscopy. The survey spectra of A33E and A33E-Ce(III) before and after the As(V) adsorption are presented in Fig. 6a which reveals the presence of Fe, O, N and C in all samples. The main forms of iron and oxygen are iron(II,III) oxides Fe_xO_y . Nitrogen occurs mainly as the quaternary ammonium groups while carbon results from the presence of the aliphatic C-H, aliphatic C-C and aromatic C=C bonds derived from polystyrene crosslinked with divinylbenzene. In the survey spectrum of A33E-Ce(III) the Ce peak appears which proves successful adsorption with the cerium(III) ions. Moreover, the As peaks indicate that the arsenate adsorption could proceed on both modified and unmodified ion exchangers. Fig. 6b and 6c presents the As3d region in the range of 48-42 eV. It can be seen that in the case of A33E-Ce(III) the As peaks are shifted and have different intensities compared to A33E. This suggests various mechanisms of arsenate adsorption on the tested materials. Interestingly, in the As3d region the peaks originating from As(III) appear. This can be explained by the susceptibility of As(V) ions to the reduction induced by X-rays during the XPS analysis. For instance, Viltres et al. proved that As_2O_5 is degraded due to the XPS measurements and this damage involves the reduction of As(V) to As(III) species along with oxygen losses from the oxide surface (Viltres et al., 2020). In the case of the Ce3d region (Fig. 6d and 6e), the cerium peaks were also shifted and their intensity decreased after the adsorption of As(V) ions. This suggested that cerium was involved in the process of arsenate adsorption. It is worth noting that after the adsorption of cerium(III) ions on A33E, they were partially oxidized to cerium(IV) ions. This phenomenon can be explained by converting Ce(III) into Ce(IV) ions under the influence of oxidants such as oxygen during the preparation process of the Ce-modified material (He et al., 2012).

3.2. Effect of pH

The influence of solution pH on the arsenate adsorption was investigated over a pH range of 4-11. As illustrated in Fig. 7, when the solution pH increases from 4 to 6, the adsorption of arsenate on A33E-Ce(III) is slightly boosted, and the maximum adsorption capacity of 19.6 mg/g is achieved at pH 6. The arsenate adsorption onto A33E-Ce(III) decreases as the solution pH rises.

Based on the arsenic speciation diagram presented by Issa et al., the main arsenate species in the pH range of 4 to 11 are H_2AsO_4^- and HAsO_4^{2-} (Issa et al., 2011). Electrostatic interactions between the adsorbent active sites and arsenate may be critical in the adsorption process. Due to the fact that the pH_{PZC} of the adsorbent is 8.12, stronger protonation of the functional groups on its surface can be achieved at the pH values less than 8.12, resulting in the enhanced electrostatic attraction between the adsorbent positively charged active sites and the negatively charged arsenate (Li et al., 2011), as shown in Eqs. 19 and 20.



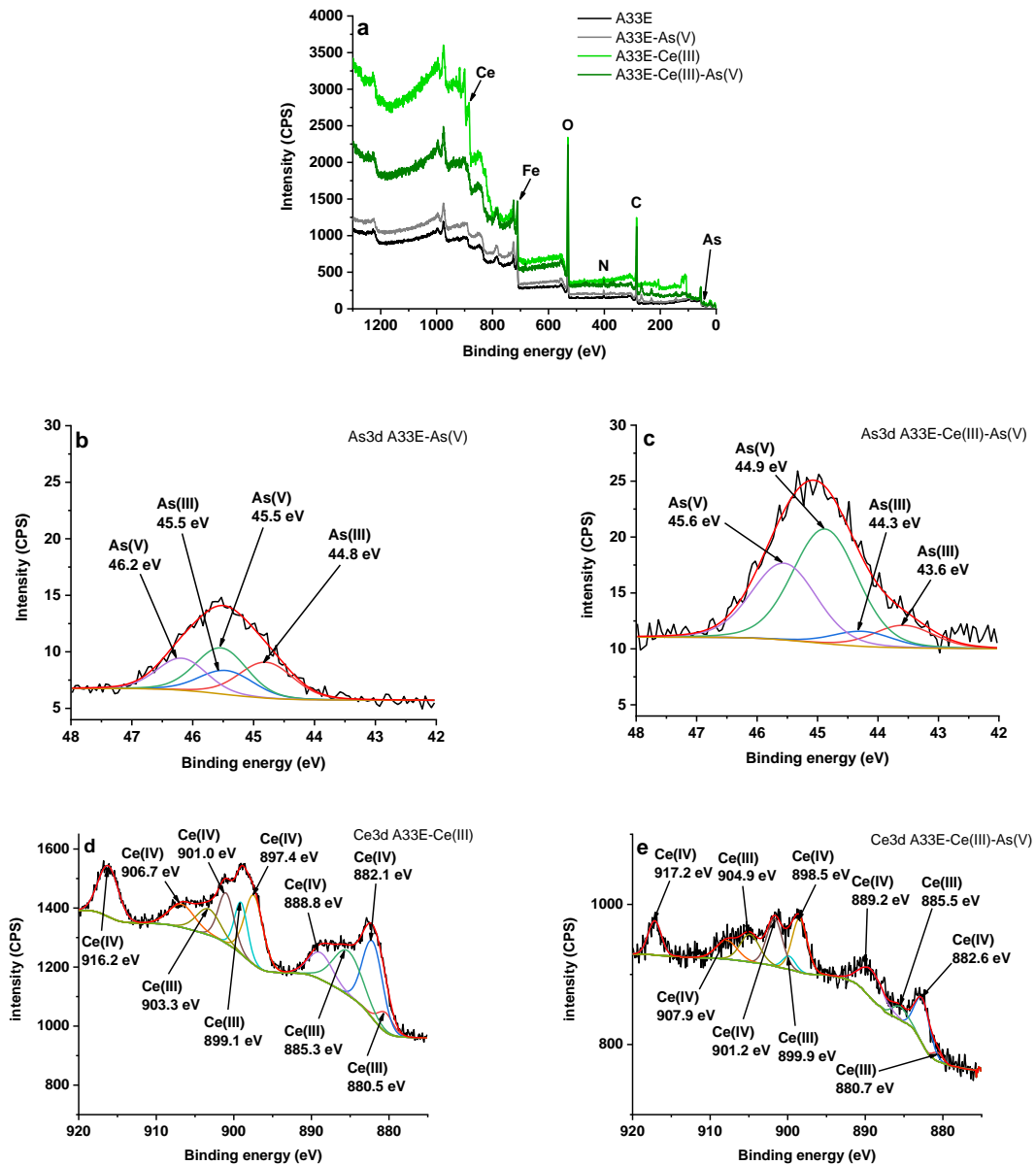


Fig. 6. XPS survey spectra of A33E, A33E-As(V), A33E-Ce(III), A33E-Ce(III)-As(V) (a), As3d region of A33E-As(V) (b), As3d region of A33E-Ce(III)-As(V) (c), Ce3d region of A33E-Ce(III) (d) and Ce3d region of A33E-Ce(III)-As(V) (e)

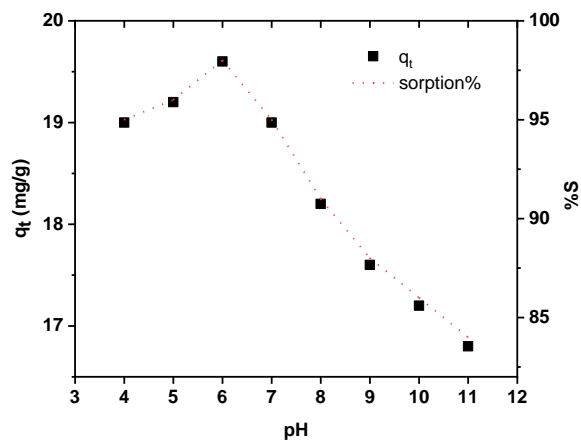


Fig. 7. Influence of pH on the adsorption efficiency of As(V) on A33E-Ce(III) (initial As(V) concentration c_0 100 mg/dm³, time t 360 minutes, shaking speed 180 rpm, temperature T 295 K)

Moreover, the FTIR analysis revealed the formation of a new Ce-O-As bond. This indicates formation of the monodentate and bidentate surface complexes (Peng et al., 2005) which is presented in Fig. 8.

Though adsorption of As(V) was still possible at alkaline pH, the sorption efficiency was significantly reduced. When the pH of the adsorbent exceeds 8.12, the electrostatic repulsion effect limits considerably arsenate adsorption (Nabi et al., 2009).

It should be noted that the batch adsorption studies were carried out with the model solutions containing only arsenate(V) ions. When removing arsenic from natural waters, the influence of accompanying ions should be taken into account. Largely present Cl^- , SO_4^{2-} , Na^+ and K^+ ions do not show any significant effect on the arsenate(V) adsorption. Ca^{2+} and Mg^{2+} ions exhibit even promoting effects on the arsenic removal. However, both phosphate PO_4^{3-} and hydrogen carbonate HCO_3^- can have a negative impact on the process. The PO_4^{3-} and HCO_3^- inhibitory effects are related to competing adsorption mechanisms. Boosting action of Ca^{2+} and Mg^{2+} ions may be a consequence of electrostatic attraction, co-precipitation, and surface complexation on the porous iron-based material in aqueous solutions (Yang et al., 2015).

3.3. Kinetic studies

Fig. 9 shows the rate of adsorption of As(V) on A33E-Ce(III) and A33E at the initial concentrations of 25, 50 and 100 mg/dm^3 . As follows from this Fig. the adsorption capacities increased very fast during the first 30 minutes with the increasing contact time. Equilibrium was attained after about 30, 60 and 120 minutes for the initial concentrations of 25, 50 and 100 mg/dm^3 , respectively. It is worth noting that the time needed to achieve equilibrium did not deteriorate after the modification. Moreover, at each tested concentration, A33E-Ce(III) showed better sorption percentage than A33E. In contrast with the unmodified ion exchanger (Dudek and Kołodyńska, 2022), it could remove arsenic even completely in 60 minutes from an arsenate solution at such a high concentration as 50 mg/dm^3 .

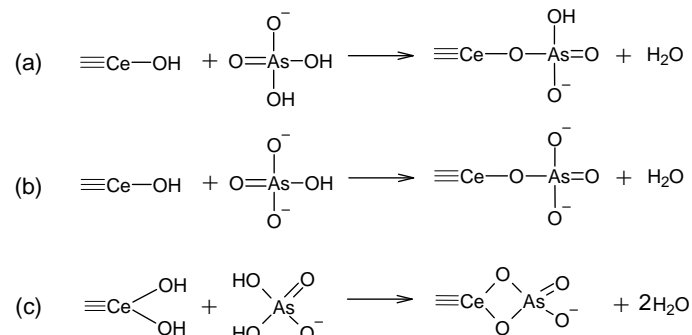


Fig. 8. Formation of monodentate (a, b) and bidentate complexes (c) by arsenate species

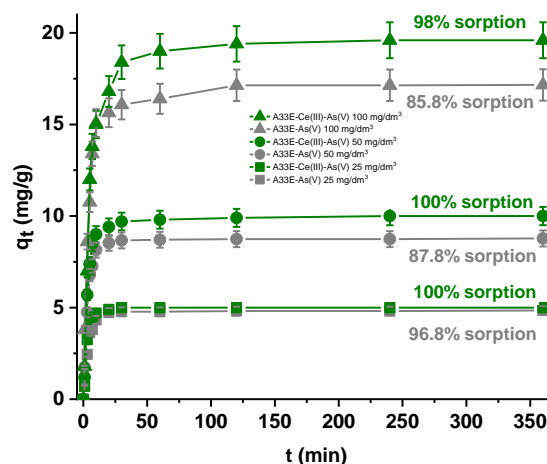


Fig. 9. Influence of As(V) initial concentration and contact time on the adsorption capacities of A33E (grey) and A33E-Ce(III) (green) (initial As(V) concentration c_0 25, 50, 100 mg/dm^3 , pH 6, time t 1-360 minutes, temperature T 295 K, shaking speed 180 rpm)

During the investigations the pseudo-first order PFO, pseudo-second order, Elovich and intraparticle diffusion models were tested for explaining the adsorption behaviour of arsenate ions on A33E-Ce(III). All kinetic parameters are presented in Table 1. Figs. 10 and S1 show the non-linear and linear fitting of the tested kinetic models in turn.

The PFO and PSO models are the most often used in the environmental kinetic studies (Guo and Wang, 2019). According to the kinetic parameters presented in Table 1 for the sorption of arsenate ions on A33E-Ce(III), the PSO model with the correlation coefficients close to one provides the best fit to the data expected from the experimental values. This is also confirmed by the SSE error analysis and indicates the chemical adsorption process (Khan et al., 2020). Moreover, the equilibrium adsorption capacities q_e obtained from the PSO model are close to the experimental data. The applicability of the PSO model was also compared with that of the Elovich model. It was noticed that the Elovich model was not well suited to fit the arsenate adsorption kinetics owing to its low R^2 and relatively high SSE values. However, the attention should be paid to the fact that numerous studies proved that adsorption behaviour that closely matches the PSO model can often be explained by the diffusion-based processes (Hubbe et al., 2019; Simonin, 2016). It has been shown that the hypothetical data obtained from the premise of pseudo-first-order rate behavior fit the PSO model quite well. According to published research, the adsorption kinetics of various materials are likely to be dominated by the diffusion-limited processes, as influenced by the heterogeneous pore size distributions and continuous partitioning of solute species between their dissolved and fixed states of adsorption.

Since the PSO model does not explain the process of adsorption diffusion, the intraparticle diffusion model (IPD) can be used to determine the rate controlling stages. The multilinear IPD plot for q_t vs $t_{1/2}$ (Fig. 10 c) indicates that three diffusion steps are involved in the As(V) adsorption on A33E-Ce(III) (Sharma et al., 2019). The first stage involves the diffusion of arsenate ions through the solution to the surface of A33E-Ce(III). The adsorption process is rapid in this stage, and the curve is steeply sloped. The intraparticle diffusion limits the reaction rate in the second stage, resulting in curve flattening. Due to reaching equilibrium and the decrease in arsenate ions concentration in the solution,

Table 1. Kinetic parameters of As(V) adsorption on A33E-Ce(III)

Model	Parameter	As(V)	As(V)	As(V)
		25 mg/dm ³	50 mg/dm ³	100 mg/dm ³
	q_e (mg/g)	5.00	10.00	19.60
PFO	q_1 (mg/g)	0.26	2.20	8.00
	k_1 (1/min)	0.029	0.030	0.035
	R^2	0.4798	0.8974	0.9631
	SSE	207.43	605.85	1346.07
PSO	q_2 (mg/g)	5.03	10.08	19.89
	k_2 (g/mg·min)	0.144	0.043	0.012
	R^2	0.9998	0.9998	0.9997
	SSE	2.45	5.42	11.28
Elovich	a (mg/g·min)	97.39	63.98	25.45
	β (g/mg)	1.92	0.86	0.36
	R^2	0.5567	0.6626	0.8134
	SSE	7.56	24.37	63.55
IPD	k_{i1} (mg/g·min ^{-1/2})	2.991	4.451	6.416
	C_1 (mg/g)	2.187	2.773	3.907
	R^2_1	0.9858	0.9641	0.9547
	k_{i2} (mg/g·min ^{-1/2})	0.206	0.303	0.603
	C_2 (mg/g)	3.994	8.044	14.511
	R^2_2	0.9408	1.0000	0.7901
	k_{i3} (mg/g·min ^{-1/2})	0.000	0.018	0.026
	C_3 (mg/g)	4.997	9.682	19.141
	R^2_3	0.5370	0.8978	0.8193
	SSE	0.10	1.12	5.97

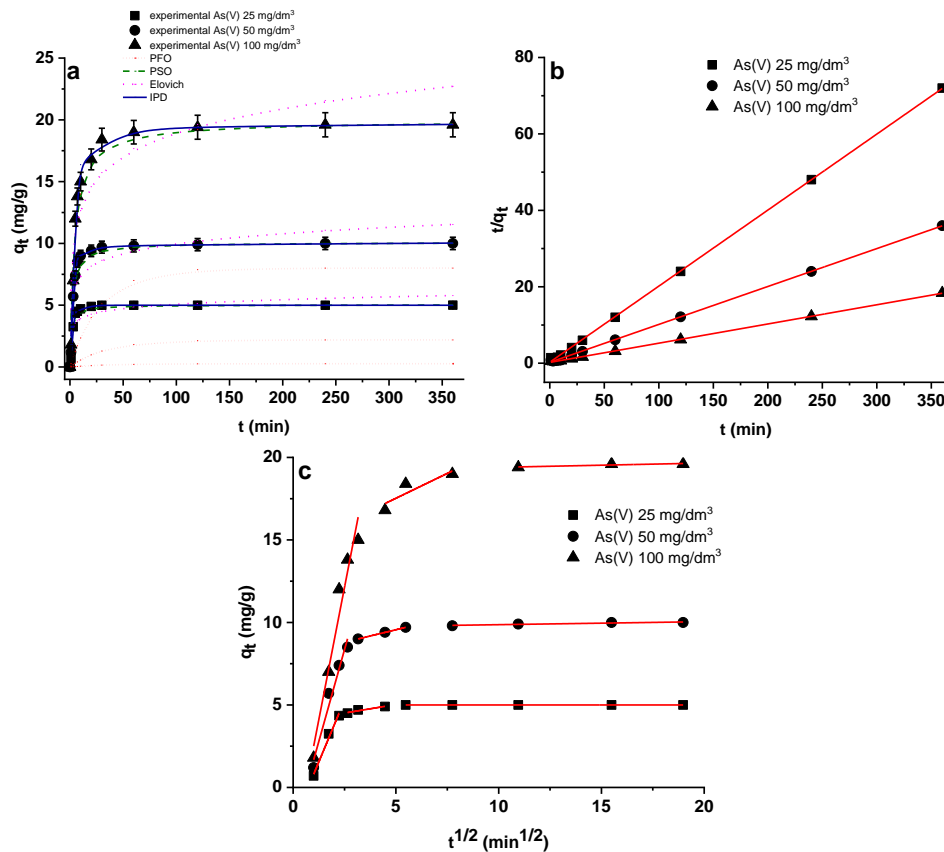


Fig. 10. Non-linear fitting of PFO, PSO, Elovich and IPD models (a) as well as linear fitting of PSO (b) and IPD (c) kinetic models related to As(V) adsorption on A33E-Ce(III) ($c_0 = 25, 50$ and 100 mg/dm³, pH = 6, shaking speed 180 rpm, temperature 295 K)

the diffusion process is inhibited (the third step). Based on the obtained values of the intraparticle diffusion rate constant, it can be deduced that these parameters decrease in the series $k_{i1} > k_{i2} > k_{i3}$. The surface gets saturated and the adsorption rate drops once the external surface is filled with arsenate ions.

3.4. Equilibrium and thermodynamic studies

The experimental data were analysed using four isotherm Eqs. (Langmuir, Freundlich, Dubinin-Radushkevich and Redlich-Peterson) to have an insight into the adsorption behaviour of arsenate ions on A33E-Ce(III) and to get the best fitting of the theoretical model. All isotherm parameters and non-linear fitting to the experimental data are presented in Table 2 and Fig. 11, respectively.

Each model is characterized by high determination coefficients ($R^2 > 0.92$), which proves their possible application in the description of the sorption process of arsenate ions on the tested ion exchanger. Based on the Langmuir model the maximum adsorption capacity for As(V) was found to be 60.41 mg/g. This indicates that the maximum sorption capacity almost doubled after the modification with cerium(III) ions. Table 3 shows the comparison of the maximum sorption capacities of various sorbents applied in the arsenic removal. It is worth noting that A33E-Ce(III) can compete successfully with other materials available on the market. The Langmuir and Freundlich models revealed that the arsenate ion adsorption on A33E-Ce(III) is a favourable and feasible process. This is evidenced by the R_L and $1/n$ factors obtained from the above-mentioned Eqs. and they were equal to 0.341 and 0.197 ($n = 5.080$), respectively.

The average sorption energies indicate whether the sorption is physical or chemical. Physical sorption occurs when the value is less than 8 kJ/mol while chemical adsorption occurs when the value is more than 8 kJ/mol (Ali et al., 2019). Based on the Dubinin-Radushkevich model the energy was equal to 18.12 kJ/mol. This confirms one of the conclusions drawn from the kinetic, XPS and FTIR studies that the process is chemical in nature.

Table 2. Langmuir, Freundlich, Dubinin-Radushkevich and Redlich-Peterson isotherm parameters with the error analysis (determination coefficients R^2 , sum of squared errors SSE and F -Test)

Parameters and error analysis	
Langmuir model	
q_m (mg/g)	60.41
K_L (dm ³ /mg)	0.077
R_L	0.341
R^2	0.997
SSE	480.89
F -Test	0.64
Freundlich model	
K_F (mg/g)	17.190
n	5.080
R^2	0.951
SSE	109.74
F -Test	0.93
Dubinin-Radushkevich model	
q_{DR} (mol/g)	$8.790 \cdot 10^{-4}$
β (mol ² /J ²)	$1.523 \cdot 10^{-9}$
E (kJ/mol)	18.12
R^2	0.928
SSE	286.85
F -Test	0.69
Redlich-Peterson model	
K_{RP} (dm ³ /g)	$9.424 \cdot 10^6$
a_{RP} (dm ³ /mg) ^g	$5.520 \cdot 10^5$
g	0.800
R^2	0.970
SSE	107.27
F -Test	0.98

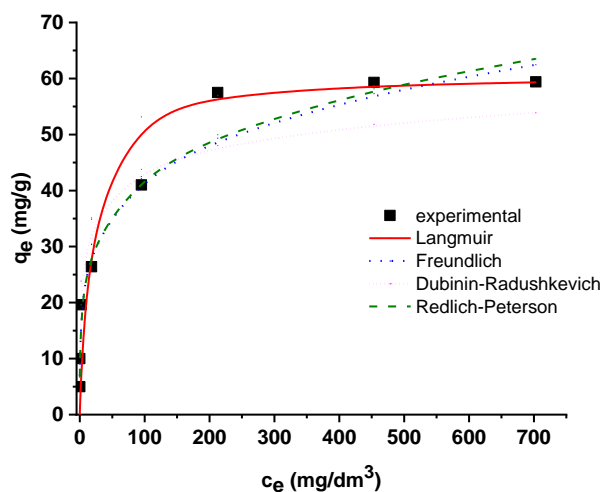


Fig. 11. Non-linear plots of the Langmuir (a), Freundlich (b), Dubinin-Radushkevich (c) and Redlich-Peterson (d) isotherm models.

Due to the fact that all determination coefficients R^2 are relatively high, a further error analysis had to be performed in order to select the best isotherm model. The sum of squared errors (SSE) and F -test revealed that the experimental data fitted best the Redlich-Peterson model which is a combination of the Langmuir and Freundlich isotherms. Due to its versatility, it describes adsorption equilibrium over

a wide range of adsorbate concentrations and is applicable to both homogeneous and heterogeneous systems. As a consequence, it was found that the As(V) adsorption on A33E-Ce(III) did not follow the ideal monolayer adsorption (Ayawei et al., 2017).

Temperature is one of the factors that impact arsenate adsorption capacity in the liquid-solid system. The temperature effect was investigated in this research at 295, 313 and 333 K. All thermodynamic parameters are given in Table 4. The negative value of the enthalpy change ($\Delta H^\circ = -3.74$ kJ/mol) indicated the exothermic process of arsenate adsorption on A33E-Ce(III). This revealed a decrease in the As(V) removal efficiency at higher temperatures (Khan et al., 2020). The findings demonstrated that the values of Gibbs free energy change (G°) were all negative at all tested temperatures. This confirmed that the adsorption process proceeded spontaneously and in a thermodynamically satisfactory manner (Dehghani et al., 2020). The positive value of the entropy change ($\Delta S^\circ = 0.0241$ kJ/mol·K) observed in this study may be attributed to the increased degree of disorderliness at the adsorbent-solution interface during the As(V) adsorption on A33E-Ce(III) (Yetilmesoy et al., 2020). Taking into account the thermodynamic studies, it is not advisable to conduct the process at elevated temperature.

Table 3. Comparison of adsorption capacities of various sorbents used for the As(V) removal

Adsorbent	As(V) adsorption capacity (mg/g)	pH	Reference
Chitosan/Cu(OH) ₂ sorbent	39.1	4.0	(Elwakeel and Guibal, 2015)
Magnate gelatin modified chestnut shell biochar	45.8	3.0-4.0	(Zhou et al., 2017)
Al-bentonite	35.71	4.0	(My Linh et al., 2019)
Hybrid anion exchange resin impregnated with hydrous zirconium oxide nanoparticles (HAIX-Zr)	20.00	7.0	(Padungthon et al., 2015)
Polymeric Al/Fe-modified montmorillonite	21.23	4.0	(Ramesh et al., 2007)
Iron-containing magnetic nanoparticles (iMNP)	12.74	6.6	(Zeng et al., 2020)
Ion exchanger based on iron oxide A33E	34.41	6.0	(Dudek and Kołodyńska, 2021)
Ion exchanger based on iron oxide modified with cerium(III) ions A33E-Ce(III)	60.41	6.0	This study

Table 4. Thermodynamic parameters

T (K)	q_e (mg/g)	c_e (mg/dm ³)	K_d (dm ³ /g)	ΔG° (kJ/mol)	ΔH° (kJ/mol)	ΔS° (kJ/mol·K)
295	59.40	703.00	0.084	-10.88	-3.74	0.0241
313	55.00	725.00	0.076	-11.27		
333	52.40	738.00	0.071	-11.80		

3.5. Reusability of A33E-Ce(III)

To evaluate the reusability of the utilized A33E-Ce(III), the regeneration with the NaOH solution and the re-adsorption of As(V) ions were examined (Zhang et al., 2014). These adsorption-regeneration cycles were repeated up to three times with the results shown in Fig. 12. After the first sorption cycle, 1M was selected as the optimal concentration of the desorbing agent. The As(V) adsorption capacity of A33E-Ce(III) reduced gradually with the increasing regeneration cycle. This decline was not so significant and after three desorptions around 92.5% of the initial adsorption capacity was still maintained. These results show that the As(V) adsorption on A33E-Ce(III) is reversible and that the exhausted ion exchanger can be successfully regenerated using NaOH. It is also worth noting that after the third desorption, A33E-Ce(III) still demonstrates greater sorption capacity than unmodified A33E before the first adsorption of arsenate ions. It should be mentioned that during the modification, the

sorption capacity for Ce(III) ions was equal to 19.74 mg/g (the initial concentration of Ce(III) solution was 100 mg/dm³). The content of cerium ions in the solution after sorption and desorption of arsenate(V) ions was checked. There was no presence of cerium, which proves the stability of loaded REE onto the sorbent during the sorption and desorption cycles.

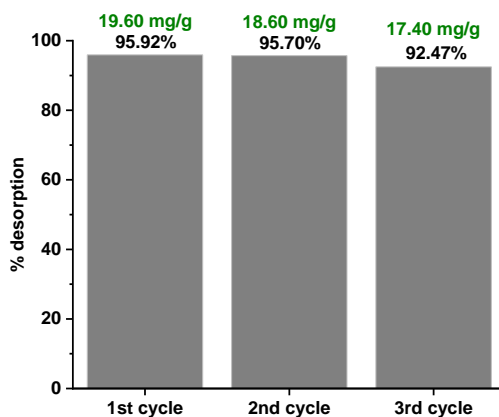


Fig. 12. Reusability of A33E-Ce(III) in the 3 consecutive cycles of sorption and desorption (initial As(V) concentration c_0 100 mg/dm³, sorption time t 360 minutes, desorbing agent 1M NaOH, desorption time t 360 minutes, pH 6, temperature T 295 K, shaking speed 180 rpm). The sorption capacities for As(V) in each cycle are marked in green

4. Conclusions

In this study the modification of the commercially available iron oxide ion exchanger Ferrix A33E (containing the quaternary ammonium groups) was successfully performed with the cerium(III) ions. This was confirmed by the SEM, FTIR and XPS analyses. In the SEM images formation of nanoflakes took place on the surface of A33E-Ce(III). The FTIR spectra revealed a new band at 448 cm⁻¹ and the XPS study found new peaks in the range of 920 and 880 eV. Compared to unmodified A33E all these changes were attributed to the presence of cerium on the sorbent surface.

The research also confirmed that the obtained material had a great affinity for the arsenate ions. According to the kinetic and isotherm models the As(V) removal process was chemisorption and it did not follow the ideal monolayer adsorption. The optimal pH for the removal of As(V) was found to be 6. Then the enhanced electrostatic attraction between the adsorbent positively charged active sites and the negatively charged arsenic species occurred. Moreover, formation of the monodentate and bidentate surface complexes took place on A33E-Ce(III). The process was exothermic, spontaneous and thermodynamically effective.

A33E-Ce(III) was characterized by much better sorption properties in relation to As(V) than A33E. In contrast with the unmodified ion exchanger, it could remove arsenic from the arsenate solution entirely at the concentration of 50 mg/dm³ in 60 minutes. Moreover, the maximum adsorption capacity for As(V) was found to be 60.41 mg/g, so it was almost doubled after the modification with cerium(III) ions. It is also worth mentioning that even after three cycles of sorption/desorption, A33E-Ce(III) still had a greater sorption capacity than unmodified A33E prior to any arsenate adsorption. It can be stated that modifying the sorbent with a small dose of cerium(III) ions increases its sorption capabilities considerably. The removal of arsenic from the aqueous solutions can be made even more effectively and low-cost. The adsorption of a small amount of cerium ions improves the efficacy of water purification significantly while reducing the total cost of the operation.

Acknowledgments

This research received no external funding.

References

- ADELOJU, S.B., KHAN, S., PATTI, A.F., 2021. *Arsenic contamination of groundwater and its implications for drinking water quality and human health in under-developed countries and remote communities – a review*. Appl. Sci. 11, 1–25.

- ALI, I., ALHARBI, O.M.L., ALOTHMAN, Z.A., ALWARTHAN, A., AL-MOHAIMEED, A.M., 2019. *Preparation of a carboxymethylcellulose-iron composite for uptake of atorvastatin in water*. *Int. J. Biol. Macromol.* 132, 244–253.
- ALOTHMAN, Z.A., 2012. *A review: Fundamental aspects of silicate mesoporous materials*. *Materials*. 5, 2874–2902.
- AYAWEL, N., EBELEGI, A.N., WANKASI, D., 2017. *Modelling and Interpretation of Adsorption Isotherms*. *J. Chem.* 2017, 3039817.
- BADRUDDOZA, A.Z.M., SHAWON, Z.B.Z., RAHMAN, M.T., HAO, K.W., HIDAJAT, K., UDDIN, M.S., 2013. *Ionicly modified magnetic nanomaterials for arsenic and chromium removal from water*. *Chem. Eng. J.* 225, 607–615.
- BERGMANN, C.P., MACHADO, F.M., 2015. *Carbon nanomaterials as adsorbents for environmental and biological applications*. Springer International Publishing, Switzerland.
- BHANDARI, P., BANJARA, M.R., SINGH, A., KANDEL, S., RAWAL, D.S., PANT, B.R., 2021. *Water quality status of groundwater and municipal water supply (tap water) from bagmati river basin in Kathmandu valley, Nepal*. *J. Water Sanit. Hyg. Dev.* 11, 102–111.
- CHAUDHRY, S.A., ZAIDI, Z., SIDDIQUI, S.I., 2017. *Isotherm, kinetic and thermodynamics of arsenic adsorption onto iron-zirconium binary oxide-coated sand (IZBOCS): Modelling and process optimization*. *J. Mol. Liq.* 229, 230–240.
- CHOWDHURY, M.R.I., MULLIGAN, C.N., 2011. *Biosorption of arsenic from contaminated water by anaerobic biomass*. *J. Hazard. Mater.* 190, 486–492.
- DEHGHANI, M.H., YETILMEZSOY, K., SALARI, M., HEIDARINEJAD, Z., YOUSEFI, M., SILLANPÄÄ, M., 2020. *Adsorptive removal of cobalt(II) from aqueous solutions using multi-walled carbon nanotubes and γ -alumina as novel adsorbents: Modelling and optimization based on response surface methodology and artificial neural network*. *J. Mol. Liq.* 299, 112154.
- DUDEK, S., KOŁODYŃSKA, D., 2022. *Arsenate removal on the iron oxide ion exchanger modified with neodymium(III) ions*. *J. Environ. Manage.* 307, 114551.
- DUDEK, S., KOŁODYŃSKA, D., 2021. *Arsenic(V) removal on the lanthanum-modified ion exchanger with quaternary ammonium groups based on iron oxide*. *J. Mol. Liq.* 347, 117985.
- DUDEK, S., KOŁODYŃSKA, D., 2020. *Enhanced arsenic(V) removal on an iron-based sorbent modified by lanthanum(III)*. *Materials*. 13, 2553.
- DUTTA, P.K., RAY, A.K., SHARMA, V.K., MILLERO, F.J., 2004. *Adsorption of arsenate and arsenite on titanium dioxide suspensions*. *J. Colloid Interface Sci.* 278, 270–275.
- ELWAKEEL, K.Z., GUIBAL, E., 2015. *Arsenic(V) sorption using chitosan/Cu(OH)₂ and chitosan/CuO composite sorbents*. *Carbohydr. Polym.* 134, 190–204.
- GUO, X., WANG, J., 2019. *A general kinetic model for adsorption: theoretical analysis and modeling*. *J. Mol. Liq.* 288, 111100.
- GUPTA, K., GHOSH, U.C., 2009. *Arsenic removal using hydrous nanostructure iron(III)–titanium(IV) binary mixed oxide from aqueous solution*. *J. Hazard. Mater.* 161, 884–892.
- HAO, L., LIU, M., WANG, N., LI, G., 2018. *A critical review on arsenic removal from water using iron-based adsorbents*. *RSC Adv.* 8, 39545–39560.
- HE, Z., TIAN, S., NING, P., 2012. *Adsorption of arsenate and arsenite from aqueous solutions by cerium-loaded cation exchange resin*. *J. Rare Earths* 30, 563–572.
- HU, Q., CHEN, N., FENG, C., HU, W.W., 2015. *Nitrate adsorption from aqueous solution using granular chitosan-Fe³⁺ complex*. *Appl. Surf. Sci.* 347, 1–9.
- HUBBE, M.A., AZIZIAN, S., DOUVEN, S., 2019. *Implications of apparent pseudo-second-order adsorption kinetics onto cellulosic materials: A review*. *BioRes.* 14, 7582–7626.
- ISSA, N.B., RAJAKOVIĆ-OGNJANOVIĆ, V.N., MARINKOVIĆ, A.D., RAJAKOVIĆ, L. V., 2011. *Separation and determination of arsenic species in water by selective exchange and hybrid resins*. *Anal. Chim. Acta* 706, 191–198.
- JIAO, Y., HAN, D., LU, Y., RONG, Y., FANG, L., LIU, Y., HAN, R., 2017. *Characterization of pine-sawdust pyrolytic char activated by phosphoric acid through microwave irradiation and adsorption property toward CDNB in batch mode*. *Desalin. Water Treat.* 77, 247–255.
- KHAN, M.A., ALQADAMI, A.A., WABAIDUR, S.M., SIDDIQUI, M.R., JEON, B.H., ALSHAREEF, S.A., ALOTHMAN, Z.A., HAMEDELNIEL, A.E., 2020. *Oil industry waste based non-magnetic and magnetic hydrochar to sequester potentially toxic post-transition metal ions from water*. *J. Hazard. Mater.* 400, 123247.
- KOMNITSAS, K., ZAHARAKI, D., BARTZAS, G., ALEVIZOS, G., 2017. *Adsorption of scandium and neodymium on biochar derived after low-temperature pyrolysis of sawdust*. *Minerals* 7, 1–18.
- LI, Z., QU, J., LI, H., LIM, T.C., LIU, C., 2011. *Effect of cerium valence on As(V) adsorption by cerium-doped titanium dioxide adsorbents*. *Chem. Eng. J.* 175, 207–212.

- LIANG, S., WANG, H., LI, Y., QIN, H., LUO, Z., HUANG, B., ZHAO, X., ZHAO, C., CHEN, L., 2020. *Rare-earth based nanomaterials and their composites as electrode materials for high performance supercapacitors: A review*. *Sustain. Energy Fuels* 4, 3825–3847.
- LIANG, T., LI, L., ZHU, C., LIU, X., LI, H., SU, Q., YE, J., GENG, B., TIAN, Y., SARDAR, M.F., HUANG, X., LI, F., 2020. *Adsorption of As(V) by the novel and efficient adsorbent cerium-manganese modified biochar*. *Water* 12, 2720.
- LINGAMDINNE, L.P., KODURU, J.R., CHANG, Y.Y., KANG, S.H., YANG, J.K., 2019. *Facile synthesis of flowered mesoporous graphene oxide-lanthanum fluoride nanocomposite for adsorptive removal of arsenic*. *J. Mol. Liq.* 279, 32–42.
- LINH, N.L.M., HOANG VAN, D., DUONG, T., TINH, M.X., KHIEU, D.Q., 2019. *Adsorption of arsenate from aqueous solution onto modified Vietnamese bentonite*. *Adv. Mater. Sci. Eng.* 2019, 2710926.
- MAJI, S., GHOSH, AYAN, GUPTA, K., GHOSH, ABIR, GHORAI, U., SANTRA, A., SASIKUMAR, P., GHOSH, U.C., 2018. *Efficiency evaluation of arsenic(III) adsorption of novel graphene oxide@iron-aluminium oxide composite for the contaminated water purification*. *Sep. Purif. Technol.* 197, 388–400.
- MINO, L., NEGRI, C., SANTALUCIA, R., CERRATO, G., SPOTO, G., MARTRA, G., 2020. *Morphology, surface structure and water adsorption properties of TiO₂ nanoparticles: A comparison of different commercial samples*. *Molecules* 25, 4605.
- MUTHU PRABHU, S., CHUAICHAM, C., SASAKI, K., 2018. *A mechanistic approach for the synthesis of carboxylate-rich carbonaceous biomass-doped lanthanum-oxalate nanocomplex for arsenate adsorption*. *ACS Sustain. Chem. Eng.* 6, 6052–6063.
- MUTHUSELVI, M., JEYASUBRAMANIAN, K., HIKKU, G.S., MUTHUSELVAN, M., ESWARAN, M., SENTHIL KUMAR, N., PONNUSAMY, V.K., 2021. *Rare earth metal oxide-doped reduced graphene-oxide nanocomposite as binder-free hybrid electrode material for supercapacitor application*. *Int. J. Energy Res.* 45, 8255–8266.
- NABI, D., ASLAM, I., QAZI, I.A., 2009. *Evaluation of the adsorption potential of titanium dioxide nanoparticles for arsenic removal*. *J. Environ. Sci.* 21, 402–408.
- PADUNGTHON, S., GERMAN, M., WIRIYATHAMCHAROEN, S., SENGUPTA, A.K., 2015. *Polymeric anion exchanger supported hydrated Zr(IV) oxide nanoparticles: A reusable hybrid sorbent for selective trace arsenic removal*. *React. Funct. Polym.* 93, 84–94.
- PENG, X., LUAN, Z., DING, J., DI, Z., LI, Y., TIAN, B., 2005. *Ceria nanoparticles supported on carbon nanotubes for the removal of arsenate from water*. *Mater. Lett.* 59, 399–403.
- PODGORSKI, J.E., EQANI, S.A.M.A.S., KHANAM, T., ULLAH, R., SHEN, H., BERG, M., 2017. *Extensive arsenic contamination in high-pH unconfined aquifers in the Indus Valley*. *Sci. Adv.* 3, 1700935.
- RAMESH, A., HASEGAWA, H., MAKI, T., UEDA, K., 2007. *Adsorption of inorganic and organic arsenic from aqueous solutions by polymeric Al/Fe modified montmorillonite*. *Sep. Purif. Technol.* 56, 90–100.
- RAVI, PANDEY, L.M., 2019. *Enhanced adsorption capacity of designed bentonite and alginate beads for the effective removal of methylene blue*. *Appl. Clay Sci.* 169, 102–111.
- REID, M.S., HOY, K.S., SCHOFIELD, J.R.M., UPPAL, J.S., LIN, Y., LU, X., PENG, H., LE, X.C., 2020. *Arsenic speciation analysis: A review with an emphasis on chromatographic separations*. *TrAC - Trends Anal. Chem.* 123, 115770.
- SHARMA, M., SINGH, J., HAZRA, S., BASU, S., 2019. *Adsorption of heavy metal ions by mesoporous ZnO and TiO₂@ZnO monoliths: Adsorption and kinetic studies*. 145, 105–112.
- SHI, Q., YAN, L., CHAN, T., JING, C., 2015. *Arsenic adsorption on lanthanum-impregnated activated alumina: spectroscopic and DFT study*. *ACS Appl. Mater. Interfaces* 7, 26735–26741.
- SHIN, S.M., PARK, J.K., JUNG, S.M., 2015. *Changes of aromatic CH and aliphatic CH in in-situ FT-IR spectra of bituminous coals in the thermoplastic range*. *ISIJ Int.* 55, 1591–1598.
- SIDDIQUI, S.I., CHAUDHRY, S.A., 2017. *Iron oxide and its modified forms as an adsorbent for arsenic removal: A comprehensive recent advancement*. *Process Saf. Environ. Prot.* 111, 592–626.
- SIMONIN, J.P., 2016. *On the comparison of pseudo-first order and pseudo-second order rate laws in the modeling of adsorption kinetics*. *Chem. Eng. J.* 300, 254–263.
- VALDÉS, O., MARICAN, A., MIRABAL-GALLARDO, Y., SANTOS, L.S., 2018. *Selective and efficient arsenic recovery from water through quaternary amino-functionalized silica*. *Polymers.* 10, 626.
- VILTRES, H., ODIO, O.F., LARTUNDO-ROJAS, L., REGUERA, E., 2020. *Degradation study of arsenic oxides under XPS measurements*. *Appl. Surf. Sci.* 511, 145606.
- WANG, Y., LIU, Y., GUO, T., LIU, H., LI, J., WANG, S., LI, X., WANG, X., JIA, Y., 2020. *Lanthanum hydroxide: a highly efficient and selective adsorbent for arsenate removal from aqueous solution*. *Environ. Sci. Pollut. Res.* 27, 42868–42880.
- WANG, Y., SHI, W., YU, Y., CHEN, X., 2009. *Synthesis, characterization and properties of quaternary ammonium cationic cellulose*. 3rd International Conference on Bioinformatics and Biomedical Engineering. 1–4.

- XIAO, X., PENG, B., CAI, L., ZHANG, X., LIU, S., WANG, Y., 2018. *The high efficient catalytic properties for thermal decomposition of ammonium perchlorate using mesoporous ZnCo₂O₄ rods synthesized by oxalate co-precipitation method.* Sci. Rep. 8, 1–13.
- XIONG, F., HWANG, B., JIANG, Z., JAMES, D., LU, H., MOORTGAT, J., 2021. *Kinetic emission of shale gas in saline water: Insights from experimental observation of gas shale in canister desorption testing.* Fuel 300, 121006.
- XU, N., RATE, A.W., MORGAN, B., SAUNDERS, M., 2019. *Micro- and nanoscale identification of rare earth element-mineral associations in an acidified dredge spoil and adjacent reduced sediments.* ACS Earth Sp. Chem. 3, 51–61.
- YANG, G., LIU, Y., SONG, S., 2015. *Competitive adsorption of As(V) with co-existing ions on porous hematite in aqueous solutions.* J. Environ. Chem. Eng. 3, 1497–1503.
- YETILMEZSOY, K., ÖZÇİMEN, D., KOÇER, A.T., BAHRAMIAN, M., KIYAN, E., AKBIN, H.M., GONCALOĞLU, B.İ., 2020. *Removal of anthraquinone dye via struvite: equilibria, kinetics, thermodynamics, fuzzy logic modeling.* Int. J. Environ. Res. 14, 541–566.
- YU, Y., YU, L., KOH, K.Y., WANG, C., CHEN, J.P., 2018. *Rare-earth metal based adsorbents for effective removal of arsenic from water: A critical review.* Crit. Rev. Environ. Sci. Technol. 48, 1127–1164.
- YU, Y., ZHANG, C., YANG, L., PAUL CHEN, J., 2017. *Cerium oxide modified activated carbon as an efficient and effective adsorbent for rapid uptake of arsenate and arsenite: material development and study of performance and mechanisms.* Chem. Eng. J. 315, 630–638.
- ZENG, H., ZHAI, L., QIAO, T., YU, Y., ZHANG, J., LI, D., 2020. *Efficient removal of As(V) from aqueous media by magnetic nanoparticles prepared with Iron-containing water treatment residuals.* Sci. Rep. 10, 1–12.
- ZHANG, G., REN, Z., ZHANG, X., CHEN, J., 2013. *Nanostructured iron(III)-copper(II) binary oxide: A novel adsorbent for enhanced arsenic removal from aqueous solutions.* Water Res. 47, 4022–4031.
- ZHANG, R., LEIVISKÄ, T., 2020. *Surface modification of pine bark with quaternary ammonium groups and its use for vanadium removal.* Chem. Eng. J. 385, 123967.
- ZHANG, W., FU, J., ZHANG, G., ZHANG, X., 2014. *Enhanced arsenate removal by novel Fe-La composite (hydr)oxides synthesized via coprecipitation.* Chem. Eng. J. 251, 69–79.
- ZHANG, W., NIU, X., CHEN, L., YUAN, F., ZHU, Y., 2016. *Soot combustion over nanostructured ceria with different morphologies.* Sci. Rep. 6, 1–10.
- ZHOU, Z., LIU, Y., LIU, S., LIU, H., ZENG, G., TAN, X., YANG, C., DING, Y., YAN, Z. LI, CAI, X., 2017. *Sorption performance and mechanisms of arsenic(V) removal by magnetic gelatin-modified biochar.* Chem. Eng. J. 314, 223–231.